JOURNAL OF LABELLED COMPOUNDS AND RADIOPHARMACEUTICALS
J Label Compd Radiopharm 2003; **46**: 1–27.
Published online in Wiley InterScience (www.interscience.wiley.com). DOI: 10.1002/jlcr.639

Review Article

The production of a broader palette of PET tracers

R. J. Nickles*
Medical Physics Department, University of Wisconsin, Madison WI, USA

Table of contents:

*Correspondence to: R. J. Nickles, Medical Physics Department, University of Wisconsin, Room 1530 Medical Sciences Madison, WI 53706, USA.

Received 8 May 2001
Revised 17 July 2002
Accepted 24 July 2002

1. Introduction

The application of cyclotrons to medical inquiry, accompanied by the rise of positron emission tomography, has engaged a growing cadre of researchers, chemists, physicists, and clinicians. They join in a quest to bring the tracer technique to bear on the basic understanding of the disease process. The recent clinical embrace is welcomed, albeit with it's faster pace driven by the scent of revenue. There is a sharpening focus on tracers that fit into the template epitomized by [F-18]-FDG, analogues of critical bio-compounds, trapped at a rate-limiting step to reveal a key process. The elemental constituents of native biological compounds leads to PET labeling with a short list of radionuclides, ^{11}C, ^{13}N, ^{15}O and ^{18}F. This focus poses the threat that radionuclides off the main sequence (CNOF) may be orphaned, neglected due to unfamiliarity of production techniques, or less-than-perfect decay characteristics. This review would address that concern, casting some brief attention to the technical aspects of making a wider array of starting materials from which to fashion radiotracers capable of illuminating physiological function.

1.1. Historical benchmarks

The discovery of radioactivity has passed the century mark; the application of radioactive tracers is soon to follow. The naturally occurring radionuclides are mostly daughters along the alpha decay chains, throttled at their headwaters by a rate-limiting uranium or thorium with a half-life of cosmological scale, 10^{10} years. The arduous separation of the shorter-lived, and thus more active, decay products required remarkable perseverance,[1] in a day before chromatography and solvent extraction techniques were known. Little time passed between the isolation of radium and the application of lead-210[2] in a carefully thought-out, dynamic measurement of lead transport in plants. Soon after, the energetic alphas from polonium were used for transmutation experiments,[3] such as

$$^{27}\mathrm{Al}(\alpha, \mathrm{n})^{30}\mathrm{P}$$

with the elemental identity of the 2-min, positron-emitting phosphorous confirmed by the its chemical conversion to phosphine. It is truly humbling that the pioneers of radiochemistry made such giant strides in technique and imagination, in a time prior to the discovery of the vacuum triode which would usher in the age of electronics.

The progression of nuclear physics, and the availability of radioisotopic tracers, closely follows the development of accelerators. The cyclotron[4] and the electrostatic generator[5,6] provided charged particle beams with exquisite spatial and energy control, permitting the systematic production of a wide variety of products. It is little realized that the biological sciences made extensive use of 20-min carbon-11 in the pre-war years, with a rich literaure[7] covering topics that were not rediscovered until 40 years later.

Post-war access to nuclear reactors gave rise to longer-lived carbon-14, tritium, P-32 and S-35, which allowed the bench chemist to conduct his tracer studies at a more relaxed pace. Reactors consume kilograms of fissile fuel, making moles of neutrons with fluxes of the order of 10^{13-15} n/s-cm^2. Thermal neutron capture cross sections are of the order of barns, rather than mbarn for typical charged particle reactions. Finally, target thicknesses can be g/cm^2, a thousand-fold greater than charged particle ranges. This typically results in kCi activities from reactors, rather than mCi from most accelerators. This 6-decade scale-up in feedstock opened the doors for the large-scale application of radiotracers in medicine, biology, industry[8] and agricultural science.[9–11] Clearly, the same advantages that radionuclide imaging brings to medicine, namely non-invasiveness, tracer authenticity and mass-less concentrations, can bear fruit in other disciplines as well.

The last four decades of the medical application of radiotracers have been shaped by the symbiotic development[12] of imaging instruments (e.g. the Anger camera) and the concurrent rise of agents labeled with ideal imaging characteristics, most notably ^{99m}Tc.[13] It is a credit to technetium chemists that, starting with an element that is not native to our solar system, such a wide array of useful radiopharmaceuticals could be fashioned.

1.2. PET returns to biochemistry

The logical sequence that underlies PET's appeal to the biological scientist is grounded in three overwhelming virtues. First, its tracers are authentic, with the pivotal elements of carbon, nitrogen, oxygen and hydrogen respectively represented by the radioactive ^{11}C, ^{13}N, ^{15}O and the stand-in ^{18}F. Second, the measurements are non-invasive, with quantitative, *in vivo* imaging in transverse section isolation with spatial resolution on the millimeter scale. And finally, the studies do not perturb the microsystem, being possible at true tracer concentrations below any pharmacological threshold. The high specific activities are a direct consequence of charged particle transmutation ($\Delta Z = \pm 1$) and the short physical half-lives, offsetting their logistical disadvantages.

In the conventional wisdom, the four PET tracers, ^{11}C, ^{13}N, ^{15}O and ^{18}F, form the basic inventory from which to synthesize imaging agents to trace the body's metabolic pathways. However, this review would invert the cornucopia, deferring any judgment until all of the candidates are shaken out. From this broader perspective, we then select the pearls from those precursor radioisotopes that we can actually make. Magnesium-28, iron-52 and copper 67 exert a siren's song, with a perfect fit to important measurements of physiological function. But their inaccessibility to all but the largest accelerators places them effectively out of reach. We should focus our attentions on those products that could lie within our grasp, limited by fluxes in real reactors and beams from real accelerators. Even the smallest cyclotron dedicated to PET proves to be amazingly versatile, capable of providing mCi levels of dozens of radioisotopes up to the rare earths. With these tracers, we can prime the pump for radiopharmaceutical development, provide tracers for 'working applications' in industry, agriculture and nutritional applications, as well as providing labeled agents for translational basic research.

Examples of these translational investigations include the autoradiographic imaging of Rhizobial $^{13}N_2$-fixation[14,15] and mitochondrial ^{15}O-oxydative phosphorylation[16] where the demands for spatial and temporal resolution surpass even the most challenging PET studies of today.

Finally, nuclear astrophysicists study the reactions that occur in the violence of supernovae, where a ten billion year-old star is playing out its last hundred seconds, releasing a major fraction of its stellar mass as radiation and alpha condensates. The 'hot CNO cycle' precedes this finale, where rapid proton accretion on ^{12}C leads to ^{14}O. This 71-s oxygen, bathed in a flux of energetic alphas, can enter into a breakout reaction,

$$^{14}O(\alpha, p)^{17}F$$

vaulting over the ^{16}O turning point that had limited nucleo-genesis during eons of hydrogen-burning on the main sequence. To study the details of such reactions under controlled laboratory conditions, physicists need prodigious activities of feedstock to make radioactive ion beams (RIB's) in dual-accelerator experiments. It is not a coincidence that rapid proton burning in stellar interiors pass through the very same radionuclides that PET requires. Both fields, PET and nuclear astrophysics, have benefited from the high yield product ion of ^{11}C[17], ^{13}N[18] and ^{18}F[19].

These examples remind us that radioactively labeled tracers have a rich history of application in a far-wider reach of disciplines than medicine. A clear lesson should be to keep an open mind, and welcome these parallel fields for the leavening of spirit that they provide. The basic 'nuts and bolts' discussion below runs the risk of being sophomoric, yet needs re-visiting as the recent explosion of clinical PET brings in those unfamiliar with the successes and mistakes of the past.

2. Technical considerations in the production of proton rich tracers

The chart of the nuclides[20] distills the essential details of stable and radioactive isotopes, ordered in a two-dimensional plane with neutron number N along the abscissa, and atomic number Z along the ordinate. If we expand the chart into the third dimension to reflect the (log) half-life for physical decay, Figure 1 provides this overview of decay systematics, in the limited range of $0 < Z < 20$. This departure from a binary, hot-or-not, picture of radioactivity allows for a sense of nuance, or gray scale, inviting a search for the best match between decay rate and biological kinetics at $10^1 < t_{1/2} < 10^5$ s.

2.1. Theoretical predictions

The binding energy systematics that determine the topography of the valley of beta stability are embodied in the basic form of the Myers–Swiatecki mass formula,[21] balancing the attractive and disruptive contributions to the binding energy of a charged liquid drop arising from volume, surface, Coulomb and pairing effects. The quadratic dependence on the atomic number Z of Equation (2)–(5) of Reference[21] imparts the parabolic shape on the canyon walls.[22] The physicist plays the role of an Alpine climber, judiciously choosing his path to the desired destination, a small ledge perched ≈ 8 MeV above the valley floor for each neutron dislodged.

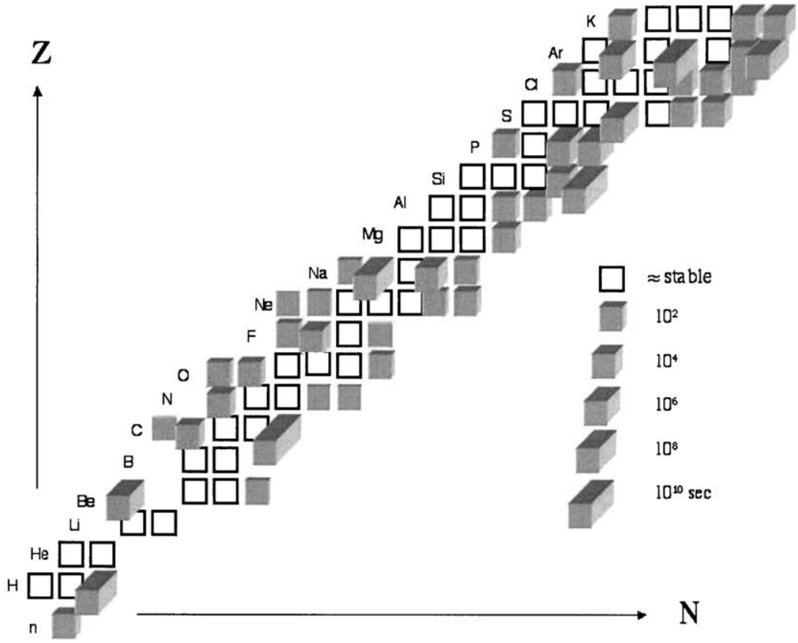

Figure 1 A graphic rendition of the valley of beta stability, from $0 < Z < 20$, showing the decay half lives in depth perspective in log scale

A useful theoretical prediction of the reaction yield is given by the code ALICE,[23] which assumes that the reaction proceeds purely through the compound nucleus

$$X + a -> C -> Y + b$$

in a two-step mechanism, formation of the compound nucleus, followed by the evaporation into product particles. The first process depends on incoming energy through its penetration of Coulomb and centrifugal barriers. The second process is characterized by the partial widths and level density of final states in the residual nucleus. Approximating these variables from the Fermi gas model leads to equations in closed form, albeit with major considerations neglected. In particular, contributions from direct reactions are not included, nor resonance reactions that account for the fine structure in the reaction cross section $\sigma(E)$, defined as the probability of the reaction occurring per target nucleus per unit beam flux. These shortcomings limit the credibility of ALICE predictions of absolute yields, but they still provide valuable insight into the competition between various allowable exit channels, which dictate the radionuclide purity of the product. The smooth energy dependence of the actual yield curve is well predicted, and can guide the experimentalist when such landmark compendia as Landolt-Bornstein[24] are silent.

2.2. Practical consequences affecting yields

Inspection of the yields of such reaction processes as

$$X(\mathrm{p},n)Y \quad \text{or } X(\mathrm{p},\alpha)Z \tag{1}$$

show that the cross section $\sigma(E)$ climbs steeply as the incident energy rises above threshold, then peaks and begins a descent at $\approx 10\,\mathrm{MeV}$ above threshold, where additional exit channels (e.g. ((p,2n), (p,αn)) open up to compete for the available flux in the entrance channel. After the reaction $X(a,b)Y$ is chosen, the best bombarding energy incident on the target can be deduced.

This exercise in variational calculus underlines the search for the accelerator best suited to make any given set of radionuclides. The result determines whether multiparticle capability is essential, or what incident beam energy E_0 is needed so that the desired activity A_0 can be achieved in an acceptable irradiation time T with a realistic beam current I. Clearly, one size does not fit all. The search must start with a realistic institutional self perception, recognizing that there is no need to be able to produce every radionuclide *on-site*. Globalization in isotope supply means that the ratio between activity A needed at the user site and the activity A_0 produced at end of irradiation at some distant production site is given by

$$A/A_0 = \exp(-\lambda \times \text{range/velocity}) \tag{2}$$

For $A/A_0 < 1$, this relation sets the range which can separate a producer from the consumer, and explicitly involves the match between the cyclotron's capability and the user's real needs. On the other hand, $A/A_0 > 1$ implies a negative range, a clear signal of unrealistic expectations, such as the widespread use of ^{67}Cu for therapy.

A figure of merit approach maximizes a rational function, representing the best "bang/buck." The numerator would favor high yields of the desired set of radionuclides. The denominator would disfavor high startup (offset) costs and elevated operating budgets. The yields are subject to the immutable laws of physics. The economics contain the vagaries of local politics. The yield is given by the integral (over energy) of the cross section σ times the target thickness $n\,\mathrm{d}x$, divided by the particle stopping power,

$$A_0 \approx I \int_0^{E_0} (\sigma/\mathrm{d}E/\mathrm{d}x) n\,\mathrm{d}x. \qquad (3)$$

This expression clearly favors:

- refractory targets that can tolerate high beam currents without destruction,
- reactions with a large cross section σ, principally involving neutron evaporation,
- high natural isotopic abundance, favoring odd-Z targets, and
- low stopping power of the incident beam, with $\mathrm{d}E/\mathrm{d}x$ going as the particle z^2.

The economic denominator of the figure of merit favors naturally abundant targets, since isotopic enrichment by electromagnetic separation generally results in material costs of the order of ten $ US per milligram. If the beam strike covers a cm^2 and target thicknesses are of the order of 100 mg/cm^2, then a thousand dollar target inventory is at stake. Post-irradiation recycling becomes mandatory, imposing tight constraints on the initial chemical steps. ^{10}B and ^{13}C are notable exceptions, where enrichment costs are driven down ($\approx$ $100/g) by gaseous diffusion on hydrides, satisfying the large demand that exists.

The scaling of accelerator cost with energy is covered by Schaarf.[25] Simple power laws govern the cost of cyclotron magnet steel and copper conductor, going as mass $\approx E^{3/2}$. A technical breakthrough, such as the strong vertical focussing inherent in deep-valley cyclotrons, permits a threefold reduction in the vertical dimension of the magnet gap, with a dramatic reduction in steel, copper, power and cooling requirements.

2.3. ^{124}I as an example

These cost/benefit factors can be seen in an extreme case. There is an increasing demand for ^{124}I as a positron emitting iodine, suitable for a wide variety of biological tracers. Two reaction pathways present themselves:

$$^{124}\mathrm{Te(p,n)}^{124}\mathrm{I} \quad \text{and} \quad ^{\mathrm{nat}}\mathrm{Sb}(\alpha,\mathrm{n})^{124}\mathrm{I}$$

Since the 4.2 day half life of ^{124}I readily permits air transport to anywhere in the world, the production of this isotope should naturally fall to a few laboratories willing to provide the service for a fair return. The first reaction can well employ a modern PET cyclotron[26] with a proton beam of 10–20 MeV, irradiating an enriched ^{124}Te oxide target. Roughly one hundred such cyclotrons populate PET centers today, but the recent explosion of clinical studies has most sites making ^{18}FDG for oncology studies virtually non-stop, with precious little beam time available for long-term irradiation of low yield reactions. Furthermore, only a few[27] are ready to invest a beam port and target inventory ($\approx$ \$20/mg ^{124}Te) that act as a ten k\$ startup cost, even with rigorous recycling.

On the other hand, many older cyclotrons, particularly in the eastern bloc, have very serviceable alpha beams. Irradiation of natural antimony was the original means[28] of making ^{123}I, albeit contaminated with ^{124}I. This base of legacy cyclotrons could embrace a new mission, fueling the world's needs for ^{124}I in exchange for much-needed foreign currency to revitalize their basic research sector. The criterion of radionuclidic purity determines the balance point. If a user insists on very low levels of the contaminant ^{126}I anticipating human applications, then thin targets or enriched ^{121}antimony would be needed. On the other hand, for animal studies or basic radiopharmaceutical chemistry, the natural antimony route should suffice. Table 1 lists saturated yields on elemental targets of 100% enrichment, as well as some of the side constraints that influence the choice of production route. The disadvantageous thermal properties of tellurium (melting point, conductivity, vapor pressure) and its oxides that limit the beam power dissipation during irradiation are evident. The advantages of a vertically directed beam cannot be overstated in the irradiation of small samples of solid target material with a low melting point. Even a shallow downward deflection can suffice to keep a molten substrate from sliding

Table 1. Target properties leading to ^{124}I

	^{124}Te(p,n) ^{124}I	^{121}Sb(α,n) ^{124}I
Natural isotopic abundance	4%	60%
Cost of target material (natural)	$\approx$ \$20/mg (95%)	$\approx$ \$3/mg (95%), ≈ 0
Thick target yield @ E_0	36 mCi/μA @ 11 MeV	17 mCi/μA(p) @ 26 MeV
Target compositron	TeO_2 melt	Plated Sb on Al substrate
Melting point	449°C	630°C
Thermal conductivity	3	24
Temperature at $P = 1$ mm Hg	520	886
Need to recycle	Essential	Unnecessary if natural Sb

down a wedge-shaped support. Innovative use[29] of sloping beams and Al_2O_3 stiffening additives to the $^{124}TeO_2$ glassy melt have allowed beams to reach tens of μA, but volatile losses of both the target substrate and the iodine product are still the rate-limiting bottleneck in the cyclotron irradiation.

The choice of production route obviously must be made on the basis of what accelerator is available, and at what cost, with the 4 day half-life inviting a global perspective. This type of choice reoccurs for most of the Group VII halogens, where the production of other versatile PET tracers (^{34m}Cl, ^{76}Br) by proton irradiation confront very real challenges in dealing with molten, toxic, volatile Group VI target materials.

2.4. *Watching the pot*

2.4.1. Physical measurements. The effective use of the major laboratory resource, the cyclotron beam **I** in the yield relation (Eq. (3)), calls for a number of sensors to monitor the irradiation and its effects, from immediate to more remote. This information warrants data logging, to provide the cyclotron operator with a running commentary on the progress of the beam, the target conditions, the resulting radiation and the activity expected at end of bombardment.

2.4.1.1. Beam current. First and most obvious is the beam current itself, from an accelerator that is a very close approximation to a perfect current source. The beam on target must be measured by a high quality electrometer with an internal impedance that is not compromised by any leakage current from the target to ground through spurious paths such as conducting O-rings or cooling water traces. A more subtle source of error in target current measurement is an imbalance of secondary electrons originating from slits immediately upstream, and those back-ejected from the target. This correction is assisted by re-entrant target design, fortuitous cyclotron fringe fields or more heroic efforts, such as several kV of electrostatic electron suppression. The charge integration of this beam current-on-target

$$Q = \int i\,dt \quad \text{(Coulombs)} \tag{4}$$

simultaneously with its measurement with a high impedance electrometer is not trivial electronically, but straightforward with current-to-frequency conversion and data logging.

More relevant is the 'leaky integral'

$$Q' = \int i \exp(-\lambda t)\, \mathrm{d}t \tag{5}$$

where the decay constant λ corresponds to the physical decay of the isotope being produced. Parameter Q' is the solution to the differential equation describing the growth of the product activity, decremented by decay that has occurred since the beginning of bombardment. This activity expectation can be formed analogically[30] with an $RC = 1/\lambda$ network across the integrating capacitor, with an up-down counter[31] or by utilizing more discriminating signals than beam current, as described below. The utility of performing this operational integration is to maintain an accurate prediction of the activity in the target, in spite of fluctuations in beam current $i(t)$.

The shape of the beam strike on target is readily apparent with a beam profile monitor directly upstream, by TV telemetry on thin foils or by the much-maligned 'tape-burn'. The variation of the beam profile with time, and as the beam current is raised, can be monitored by irradiation of a segmented mosaic[32] of isolated carbon rods. Finally, the irradiation of almost any metallic foil (Cu, Havar, stainless steel) results in induced activity that can be read out over a wide dynamic range with a brief exposure to a BaFBr (Ce) phosphor plate, a very useful resource in the accelerator lab.

2.4.1.2. Target temperature. The target temperature in the beam strike can be remotely monitored by an infra-red thermocouple.[33] The advantage over a conventional TC is that being out of the beam strike, it does not perturb the thermal ballistics of the target material. It does require the design of a germanium IR window into the target body, and some effort to keep the window clear of deposits of sublimed material. The measurement of target temperature is critical to the understanding of diffusion phenomena that underlie the transport of volatiles, of particular importance in the release of radionuclides of very short lifetime, such as $^{10}CO_2$ from molten $^{10}B_{2I}O_3$.[34]

A more refined analysis of the optical spectra from gas targets has been used by the Turku group[35] to identify the electronic and vibrational states of the target species in the beam path, useful in quantitating trace impurities and excited intermediates that dictate the hot atom fate of the recoiling product. This same group used laser measurement[36] of the index of refraction of the target gas to reveal the temperature profile during bombardment. These measurements explain the near-cyclone convection conditions that operate when tens of $\mu A \times 10\,MeV \approx$ hundreds of watts of beam power are dissipated in conventional cyclotron gas targets. The measured target gas pressure p averages over the local complexity, following the ideal gas law, $p = nRT/V = \rho RT$, thus concealing the spatial dependence of the temperature T, and density ρ, of the stopping material. Visually, the luminescent Bragg peak is clearly seen at the end of range of the 'banana-shaped' beam path, with a transient 'bounce' at the instant of beam introduction that reflects the elastic properties of the confined gas.

2.4.1.3. Characteristic radiations during bombardment. Neutrons: Neutrons emerge from the target chamber, signalling the reaction in progress. In the proton irradiation of ^{18}O, as $H_2^{18}O$ or $^{18}O_2$, the neutron flux leading to the low-lying states in ^{18}F overwhelms any other source, such as beam lost on slits or surfaces of the target chamber. Since one ^{18}F is created for every neutron, the observed neutron counting rate is the ideal input into the leaky integrator equation (Eq. (5)). Tracking the beam current i is useful, but does not alert the operator to problems inside the target, such as vapor voids, water loss or low enrichment, whereas watching the neutron counting rate assures us that the desired precursor ^{18}F is being formed.

Two neutron detectors are convenient for this purpose, the ^{235}U-foiled fission proportional counter[37] with a sensitivity selectable in the 10^{-4}–10^{-8} cps/n/cm^2 s range or the classical[38] BF_3-filled 'long counter', with a sensitivity several decades higher. Both have essentially quantitative neutron/gamma discrimination. The small footprint of the fission counter is ideal for mounting within the shielding of an enclosed cyclotron. Various efforts have been made to absolutely calibrate the detection efficiency against the known neutron fluence from a ^{241}Am–Be source, so as to achieve an absolute prediction of expected activity from Eq. (5), but errors of the order of a factor of two persist from the differing neutron energy spectra.

The logging of the neutron counting rate is useful even if the desired exit channel does not involve neutrons. Proton irradiation of a natural nitrogen gas target is the source of ^{11}carbon for a wide variety of organic syntheses, proceeding through the $^{14}N(p,\alpha)^{11}C$ reaction.

Simultaneously, the $^{14}N(p,n)^{14}O$ reaction is taking place in the target, with a neutron signature that is perfectly suitable for monitoring the concurrent production of ^{11}C.

These measured variables of beam power distribution, target temperature and neutron counting rate all enter into a detailed description[34] of the thermal ballistics of a molten $^{10}B_2O_3$ target, employed in the production of 19 s $^{10}CO_2$. The probability of release $\varepsilon(T)$ of $^{10}CO_2$ is determined by the diffusion out of the melt over a characteristic distance x_0, and is given by the Arrhenius relation.

$$\ln[\ln(1/\varepsilon)] = \ln(\lambda x_0^2)/D_0 + E_a/kT \quad (6)$$

arising from the one dimensional solution to the diffusion equation.

Release efficiency reaches $\approx 16\%$ at 15 μA of 11 MeV protons on a $^{10}B_2O_3$ glassy melt at $\approx 1400°C$. The log–log relationship (Eq. (6)) is confirmed experimentally, with an enthalpy of activation fitted to $\Delta H = 590R = 4.9$ kJ/mol, indicating convective effects in the melt, similar to earlier reports on iodine migration out of heated TeO_2 pellets.[39]

Gammas: The measurement of the energy spectrum with the gamma signature of a beam + target pair can be more problematic during production runs, where tens of μA on target result in radiation exposures of $\approx 10^3$ R/h. The intense neutron flux would quickly destroy a germanium spectrometer, and activate a NaI detector. Both BGO and YAP appear to be robust against the brutal conditions inside the cyclotron vault. However, several meters of distance and extensive shielding are needed to collimate the view of the target chamber against the omnipresent ≈ 8 MeV gamma flux from the (n,γ) capture events occuring in the walls of the accelerator vault. A laser-aligned BGO detector, housed in a 250 kg lead shield, subtends ≈ 10 μsr at 3 m from the target, with adequate energy resolution to identify the major gamma rays emerging from the irradiation of the thick targets listed in Table 2 below. The prompt gammas E_γ (Mev) arise predominately from inelastic proton scattering (p,p′) and alpha reactions to low-lying excited states. The delayed gammas E_γ (keV) and the ubquitous annihilation radiation observed in the relative calm following beam-off, come from the desired products, or unavoidable side channels.

The prompt gamma signal is heavily contaminated by background from the neutron capture events occurring in the laboratory walls, yet the gamma/neutron counting rate ratio is a characteristic of the each target/beam combination. Calibration of this ratio with modest beam

Table 2. Signature gamma rays during and following proton irradiation of light targets

Target	Reaction	E_γ (prompt)	E_γ (delayed)
$^{10}B_2O_3$	$^{16}O(p,p')$	7.2 MeV	719 keV (^{10}C), 478 (^{7}Be)
$^{14}N_2$	$^{14}N(p,p')$	2.31	511, 2314 (^{14}O)
$^{15}N_2$	$^{15}N(p,\alpha')^{12}C$	4.43	511 (^{15}O)
$H_2^{16}O$	$^{16}O(p,p')$	7.2	511 (^{13}N)
$H_2^{18}O$	$^{18}O(p,\alpha')^{15}N$	5.25	511 (^{15}F)
	$^{18}O(p,p')$	1.98	
^{20}Ne	$^{20}Ne(p,p')$	1.63	511 (^{17}F)

can provide a useful indicator when problems arise at higher beam currents. In particular, proton irradiation of a solid target such as a thin slice of elemental germanium provides useful activities of ^{72}As, needed for phantom work to characterize different PET scanners. Pressing the wafer against a water-cooled aluminum cold finger, cushioned with an indium conduction pad, permits beam currents of roughly five μA at 11 MeV before the Ge melts. The destruction of the target is signaled by the abrupt departure of the neutron/gamma ratio from its usual value, indicating that the beam is now no longer incident on the desired material. This effect is heightened if the beam stop is made of gold or tantalum, high Z materials with low neutron production.

Data logging of the neutron and gamma counting rates makes use of myriad personal computers, equipped with counter and A/D boards. A unified approach to this task is essential, since the same problem arises at every turn in the PET cyclotron lab, from logging dose calibrators, area monitors, radiation detectors in HPLC's, GC's and metabolite analyzers. The natural tendency to consolidate these data logging tasks into a single central computer may be ill-advised, since the various activities are separated in time and scattered in different distant labs, with a need for immediate visual feedback. A cost-effective solution in an academic setting is to utilize retired PC's, populated with a generic card set[40] running a common data acquisition program. A dozen such stations are spread out over the cyclotron, chemistry labs and PET imaging suite, with a unit cost of less than $500. Along with extensive inter-lab cabling and intercom linkups, all members of the group are kept aware of the progress of all activities in a laboratory situation that could otherwise quickly degenerate into chaos.

2.4.1.4. Characteristic radiation following bombardment. A wide variety of specialized detectors have been developed to measure the presence of radioactive products, with their sensitivities and operating features listed in Table 3. All of the radiation detectors are research instruments employing high quality electronics for their readout. An example of this is the ionization chamber filled with 10 atmospheres of xenon, read out by an electrometer[44] with 10^{-16} ampere sensitivity. When surrounded with a 200 kg lead shield, the advantage of this combination becomes apparent with a low background that permits positron source activities of 10 nCi to be quantitatively measured, with liter-sized sources in a 4π-well geometry. The massive shielding is essential to exploit this wide dynamic range in a high level cyclotron chemistry lab environment, with Ci of activity nearby.

Another re-entrant detector is made from a 20 cm diameter × 30 cm high cylinder of BC-400 plastic scintillator, with a 12 cm diameter × 25 cm deep well, suitable for the whole body assay of a rabbit. Three photomultipliers tubes are fanned into an electrometer for the 10 nCi-100 mCi measurement range. A PIN diode, calibrated against a built-in LED, extends this activity limit into the multi-Ci range.

Table 3. Process detectors

Application	Detector	Readout	Dynamic range	Ref
Process control	$CaWO_4$/PM	Electrometer	μCi–10 mCi/ml	
	NAI/PM	NIM electronics	10 nCi–10 μCi/ml	
Quantitative assay	Ar ion chamber	Electrometer	μCi–Ci	
	Xe ion chamber	Electrometer	10 nCi–Ci	
	Plastic well/PM	Electrometer	10 nCi–100 mCi	41
	NaI well/PM	NIM electronics	nCi–μCi	
	High purity Ge	NIM electronics	nCi–mCi	
Hot spot loc'n	BGO/fiber optics/PM	Electrometer	μCi–Ci	42
	CsI(T1)/PIN	Hand held DMM	mCi–Ci	
TLC	Si beta det	NIM electronics	nCi–10 μCi	
GC	NaI/NaI coinc	NIM electronics	nCi–μCi	
	Thermal conductivity	A/D	μmol/ml	
	Flame ionization	A/D	nmol/ml	
	Electron capture	Counter	sub nmoles/ml	
HPLC	NaI/NaI coinc	NIM electronics	nCi–μCi	
	UV absorption	A/D	nmol/ml	
	Conductivity	A/D	μmol/ml	
	Pulsed amperometric	A/D	nmol/ml	
	Evap light scattering	A/D	μmol/ml	
Metabolite analysis	Beta–gamma–gamma	NIM electronics	100 pCi/ml	43

At the other extreme, a 'point geometry' detector suitable for tracking multi-mCi bands migrating down a prep HPLC column is made by mounting a small disc of CsI(Tl) onto a silicon PIN diode,[45] light shielded and read through its optogalvanic response with a hand-held multimeter.[46] The simplicity, low ($400) parts cost, audio signal and bar-graph display make this detector indispensable in the PET chemistry lab.

Flow-through detectors are constructed as needed from a crib of NIM electronics, and detectors. Examples range from simple, shielded NaI spectrometers distinguishing 511 keV positron annihilation radiation from the signature gammas of Table 2 in passing eluates to the elaborate triple coincidence $\beta - \gamma - \gamma$ metabolite analyzer with its sub-nanoCi sensitivity and vanishing (10^{-2} cps) background.

The anchor in radionuclide quantitative assay is the high purity, intrinsic germanium detector, with its energy resolution (1.65 keV FWHM@ 1332 keV) capable of resolving complex mixtures of products and contaminants, over a wide dynamic range on a 3-m, shielded counting stage. The efficiency, nominally 15% at 1332 keV, is carefully calibrated at various standard geometries against NIST-traceable standard sources, from $59\,\text{keV} < E\gamma < 1886\,\text{keV}$. Other sources (^{24}Na and ^{152}Eu) with known relative intensities are splined to extend the efficiency calibration to 2750 keV. At lower energies, a Be-windowed Si(Li) X-ray spectrometer covers the 5–100 keV X-ray range, although absolute activity quantitation is much more difficult.

2.4.2. Chemical separation maneuvers

2.4.2.1. Dry distillation. Following the irradiation, the radioactive products must be separated from the target substrate, on a time scale that is set by the decay constant and the pace of the application. The techniques are dictated by the scale of the activity, and the need to conserve isotopically enriched target material. The dry distillation of $^{10}CO_2$ into a helium stream from a molten $^{10}B_2O_3$ melt during irradiation, the thermochromatographic separation of ^{94m}Tc from $^{94}MoO_3$,[47,48] or $^{123,\,124}$I from TeO_2,[49] are ready examples of fast, selective separation with minimal loss of the target feedstock. To its disadvantage, the additional stopping power of the oxygen lowers the yield, and the poor thermal properties of the oxides limit the beam current that the target tolerates without losing the desired activity to volatilization during the irradiation.

2.4.2.2. Sparging. A particularly constrained situation occurs when the simultaneous production of a matched pair of products is desired, as for example the oxygen pair $^{19}O_2/^{15}O_2$[50] or the pair of short-lived kryptons, $^{81m}K/^{79m}K$, with 13 and 55 s half-lives, respectively. Steady state equilibrium with a constant infusion of such a pair results in a relative concentration at any point in the body that is a measure of the tracer 'age' T. The limited solubility and absence of any chemical binding of krypton make lung imaging particularly easy to interpret, with a gamma camera well suited to form simultaneous planar images of the 190 and 127 keV gammas. The two radiotracers are sparged into a helium stream, bubbling through a liquid bromoform target under proton bombardment. Optimal gas transport can deliver mCi activities to a ballast tank upstream of the subject, included in the camera's field of view. Steady breathing from this gas supply results in an 'age image'.

$$T(x, y) = \boldsymbol{T} = (\lambda_1 - \lambda_2)^{-1} \ln((A_1^0/A_2^0)/(\mathbf{A}_1/\mathbf{A}_2)) \tag{7}$$

where bold type implies an (x, y) image, 1 refers to ^{81m}Kr, 2 refers to ^{79m}Kr, the null superscript refers to the ballast tank average, and the reduced decay constant $(\lambda_1 - \lambda_2) = \ln 2/17$ s. The age T ranges from 23 to 15 s as a normal subject switches from normal respiration to hyperventilation, with a remarkable uniformity from base to apex.

2.4.2.3. Wet chemistry. If wet chemistry is needed to separate the no-carrier-added product from the tens of milligrams of isotopically enriched target material, considerable care is needed to minimize inventory losses in closing the entire loop from one irradiation to the next. If the initial irradiation starts out with a metal foil, and the end stage of the solution-extraction-precipitation process results in the precious target stock as a small pile of oxide, then the micro-scale lanthanum thermite reduction in vacuo[51] can close the loop. Similarly, hydrogen reduction in an induction furnace can often return metal oxides (e.g. Fe_3O_4) back to a metallic pellet. Reforming a foil target for the next irradiation can employ a rolling mill, electroplating, evaporation or argon-sputtering, with their attendant losses. Two techniques that offer near-quantitative deposition of adherent planar films of molecular compounds, particularly multi-layer composites (e.g. $Ti_3\,^{15}N_2$/graphite), are jet vapor deposition[52] and high-voltage molecular plating from organic solvents.[53]

The production of the 23-min PET tracer $^{94m}TcO_4^-$, for kit-preparation of any number of clinical radiopharmaceuticals, provides an informative example. If the study involves laboratory animals, a 2-fold additional absorbed radiation dose from radionuclidic impurities is not a compelling concern. In this case, ^{94m}Tc can be made from the proton irradiation of a natural molybdenum foil.[54] Electrochemical dissolution and solvent extraction from base into methyl ethyl ketone (MEK) takes $\approx 10\,\text{min}$, with $\approx 70\%$ activity yield after drydown as $^{94m}TcO_4^-$. This is re-suspended in saline, ready for incorporation into the appropriate kit, much as if the pertechnetate had been eluted from a ^{99}Mo/^{99m}Tc generator.

If, on the other hand, the Tc-labeled pharmaceutical is destined for human use,[55] then the additional radiation dose is a concern. A layer of 95% enriched $^{94}MoO_3$ is deposited in the bottom of a glassy carbon crucible which forms the interior liner of the target chamber. After irradiation, the $^{94m}TcO_4^-$ can be separated by dry distillation at 900°C, or by careful dissolution into a small volume of concentrated $NH_4OH + H_2O_2$, followed by solvent extraction into MEK. In this case, the aqueous fraction is reserved, dried and fired to return the enriched $^{94}MoO_3$ for the next irradiation. In reality, recovery of greater than 80% of the starting ^{94}MO mass is quite difficult in the turmoil of making a patient dose. The truth of these wet chemistry endeavors to achieve loss-free recyling is belied by legions of small bottles, stored and labeled, '$^{94}MoO_3 < 95\%$ *probably* OK'.

3. A survey of yield results from proton irradiation at 11 MeV

A broad-brush approach to the measurement of over a hundred proton induced reactions was carried out, in order to ascertain the versatility of an 11 MeV proton cyclotron for general purpose activation. In general, target materials were of natural abundance, and elemental in nature, if possible. Beam current was kept low, of the order of one microamp, in cases where either the target material or the products were volatile. Charge integration employed a charge pump digitizer as well as digital logging. In a low-level laboratory 50 m distant from the cyclotron, the efficiency-calibrated high purity intrinsic germanium spectrometer separated the signature gammas, identifying the many products formed by (p,n), (p,α), (p,pn) and (p,αn) reactions on multi-isotopic targets. This task was made simpler with time resolved multi-channel analysis. Figure 2 shows the results of a brief irradiation of

Symbol	Isotope	Half-life	Eγ (keV)
8	^{128}I	25.0 m	442
0	^{130}I	12.4 h	418, 536, 669, 739, 1157
3	^{123}I	13.1 h	159
4	^{124}I	4.17 d	603, 723
6	^{126}I	13.0 d	389, 491, 666, 754

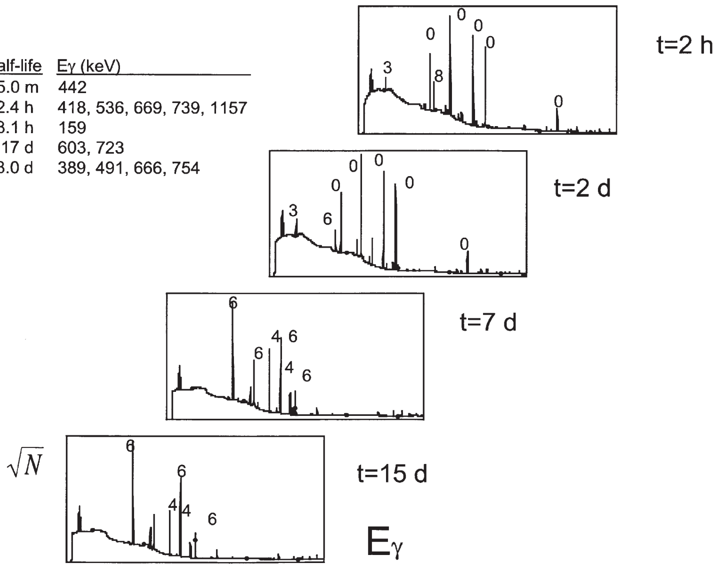

Figure 2 A sequence of high resolution gamma spectra showing the time evolution of the various radioisotopes of iodine produced by a short irradiation of natural tellurium with 11 MeV protons

natural Te, with the six iodine activities evolving over two weeks following irradiation.

In order to form a consistent basis for comparison, all measured yields are extrapolated to end-of-saturated bombardment (EOSB), and further extrapolated to the yields that would be expected from the irradiation of pure elemental targets of 100% isotopic enrichment. This facilitates the identification of those reactions that are intrinsically advantageous, beyond the fortuitous natural abundance. Finally, charge integration, secondary electron suppression and target transfer contribute to the $\pm 20\%$ uncertainties in the stated activity A, in Table 4 below, building on an earlier compendium.[56]

4. Conclusions

Several conclusions can be drawn from a re-ordering of the empirical thick target yields of Table 4. First, at least 70 of the 100 (p,n) reactions provide saturation yields above $\approx 20\,\mathrm{mCi/\mu A} \approx 10^{-5}$ reaction/proton = 10 ppm. This somewhat arbitrary watershed signals the effective

Table 4. Experimental thick target yields at $E_p = 11$ MeV at end-of-saturated-bombardment for elemental targets of 100% enrichment

Product	$t_{1/2}$	Reaction	Abund (%)	Q(Mev)	E_γ	A (mCi/μA)
^{7}Be	53 d	^{10}B(p,α)	20	+1.9	477	170
^{10}C	19 s	^{10}B(p,n)	20	−4.4	717	8
^{11}C	20 m	^{11}B(p,n)	80	−2.8	511	93
		^{14}N(p,α)	99	−2.9	511	80
^{13}N	10 m	^{13}C(p,n)	1	−3.0	511	120
		^{16}O(p,α)	99	−5.2	511	7
^{14}O	71 s	^{14}B(p,n)	99	−5.9	2314	2
^{15}O	2 m	^{15}N(p,n)	0.3	−3.5	511	70
		^{19}F(p,αn)	100	−7.5	511	1.1
^{17}F	66 s	^{20}Ne(p,α)	90	−4.1	511	14
^{18}F	2 h	^{18}O(p,n)	0.2	−2.4	511	120
^{30}P	2.5 m	^{30}Si(p,n)	3	−5.0	511	116
^{34m}Cl	32 m	^{34}S(p,n)	4	−6.4	2127	12
^{38}K	7.7 m	^{38}Ar(p,n)	0.06	−6.7	2167	5
^{43}Sc	3.9 h	^{43}Ca(p,n)	0.1	−3.0	373	11
^{44m}Sc	2.4 d	^{44}Ca(p,n)	2	−4.7	271	1.7
^{44}Sc	3.9	^{44}Ca(p,n)	2	−4.4	1157	2.9
^{48}Sc	43 h	^{48}Ca(p,n)	0.2	−0.5	984	40
^{45}Ti	3 h	^{45}Sc(p,n)	100	−2.8	511	47
^{47}V	33 m	^{47}Ti(p,n)	8	−3.8	511	100
^{48}V	16 d	^{48}Ti(p,n)	74	−4.8	1312	108
^{51}Cr	28 d	^{51}V(p,n)	99	−1.5	320	140
^{51}Mn	46 m	^{54}Fe(p,α)	6	−3.1	511	4.6
^{52m}Mn	21 m	^{52}Cr(p,n)	84	−5.9	1434	67
^{52}Mn	5.7 d	^{52}Cr(p,n)	84	−5.5	744	15
^{54}Mn	312 d	^{54}Cr(p,n)	2.4	−2.2	835	131
^{54m}Co	1.4 m	^{54}Fe(p,n)	2.4	−9.2	511	2.9
^{55}Co	17 h	^{58}Ni(p,α)	68	−1.3	931	1.3
^{56}Co	79 d	^{56}Fe(p,n)	92	−5.3	847	77
^{57}Co	271 d	^{57}Fe(p,n)	2	−1.6	122	129
		^{60}Ni(p,α)	26	−0.3	122	5.8
^{58}Co	71 d	^{58}Fe(p,n)	0.3	−3.1	811	150
^{60}Cu	23 m	^{60}Ni(p,n)	26	−6.9	1332	40
^{61}Cu	3.4 h	^{61}Ni(p,n)	1	−3.0	283	76
		^{64}Zn(p,α)	49	+0.8	283	5.2
^{62}Cu	9.8 m	^{62}Ni(p,n)	3.6	−4.7	511	130
^{64}Cu	13 h	^{64}Ni(p,n)	0.9	−2.5	511	73
^{63}Zn	38 m	^{63}Cu(p,n)	69	−4.1	669	116
^{65}Zn	244 d	^{65}Cu(p,n)	31	−2.1	115	228
^{64}Ga	2.6 m	^{64}Zn(p,n)	49	−7.9	992	10
^{66}Ga	9.4 h	^{66}Zn(p,n)	28	−6.0	1039	105
^{67}Ga	78 h	^{67}Zn(p,n)	4	−1.8	93	51
^{68}Ga	68 m	^{68}Zn(p,n)	19	−3.7	1077	177
^{69}Ge	38 h	^{69}Ga(p,n)	60	−3.0	574	103
^{70}As	53 m	^{70}Ge(p,n)	20	−7.0	1040	45
^{72}As	26 h	^{72}Ge(p,n)	27	−5.1	834	102
^{73}As	80 d	^{73}Ge(p,n)	8	−1.1	53	60
^{74}As	18 d	^{74}Ge(p,n)	36	−3.3	596	176
^{76}As	26 h	^{76}Ge(p,n)	8	−1.7	560	41
^{75}Br	95 m	^{78}Kr(p,α)	0.3	−0.1	285	0.664

Table 4. (*continued*)

^{76}Br	16 h	^{76}Se(p,n)	9	−5.4	560	37
^{77}Br	57 h	^{77}Se(p,n)	8	−2.1	239	30
^{80m}Br	4.4 h	^{80}Se(p,n)	50	−2.6	616	17
^{82}Br	35 h	^{82}Se(p,n)	9	−0.9	776	44
^{82m}Rb	6.3 h	^{82}Kr(p,n)	11	−5.2	776	15
^{83}Rb	83 h	^{83}Kr(p,n)	12	−1.6	520	23
^{84m}Rb	20 m	^{84}Kr(p,n)	57	−3.9	248	8
^{84}Rb	33 d	^{84}Kr(p,n)	57	−3.5	881	38
^{86}Rb	19 d	^{86}Kr(p,n)	17	−1.3	1076	65
^{84}Y	38 m	^{84}Sr(p,n)	0.6	−7.1	793	31
^{86}Y	15 h	^{86}Sr(p,n)	10	−6.1	1076	70
^{87m}Y	13 h	^{87}Sr(p,n)	7	−2.9	381	83
^{87}Y	80 h	^{87}Sr(p,n)	7	−2.5	485	157
^{88}Y	108 d	^{88}Sr(p,n)	83	−4.4	898	96
^{89}Zr	78 h	^{83}Y(p,n)	100	−3.6	909	100
^{90}Nb	15 h	^{90}Zr(p,n)	51	−6.9	2319	44
^{92m}Nb	10 d	^{92}Zr(p,n)	17	−2.9	934	88
^{96}Nb	23 h	^{96}Zr(p,n)	3	−0.6	778	66
^{93m}Mo	7 h	^{93}Nb(p,n)	100	−3.6	685	1.7
^{92}Tc	4 m	^{92}Mo(p,n)	15	−8.8	1510	17
^{94m}Tc	53 m	^{94}Mo(p,n)	15	−8.9	871	50
^{94}Tc	5 h	^{94}Mo(p,n)	9	−5.0	871	10
^{95m}Tc	61 d	^{95}Mo(p,n)	16	−2.5	204	21
^{95}Tc	20 h	^{95}Mo(p,n)	16	−2.4	766	50
^{96}Tc	4 d	^{96}Mo(p,n)	17	−3.7	778	95
^{99m}Tc	6 h	^{100}Mo(p,2n)	10	−7.7	140	12
^{96}Rh	10 m	^{96}Ru(p,n)	5	−7.2	833	18
^{98}Rh	9 m	^{98}Ru(p,n)	2	−5.0	652	56
^{99m}Rh	5 h	^{99}Ru(p,n)	13	−2.9	1261	40
^{99}Rh	15 d	^{99}Ru(p,n)	13	−2.9	528	18
^{100}Rh	20 h	^{100}Ru(p,n)	13	−4.4	540	63
^{101m}Rh	4 d	^{101}Ru(p,n)	17	−1.5	307	50
^{102m}Rh	206 d	^{102}Ru(p,n)	32	−3.2	478	66
^{103}Pd	17 d	^{103}Rh(p,n)	100	−1.3	20	94
^{107}Cd	6 h	^{107}Ag(p,n)	52	−2.2	824	66
^{109}Cd	453 d	^{109}Ag(p,n)	48	−1.0	88	48
^{110}In	69 m	^{110}Cd(p,n)	12	−4.7	658	179
^{111}In	2.8 d	^{111}Cd(p,n)	13	−1.9	245	54
^{112m}In	21 m	^{112}Cd(p,n)	24	−3.4	155	139
^{113m}In	1.6 h	^{113}In(p,p′)	4	−0.4	392	0.23
		^{113}Cd(p,n)	12	−0.9	392	143
^{114m}In	49 d	^{114}Cd(p,n)	29	−2.4	725	5.5
^{115m}In	4 h	^{115}In(p,p′)	95	−0.3	336	0.18
^{113m}Sn	21 m	^{113}In(p,n)	4	−2.0	79	4.3
^{116m}Sb	60 m	^{116}Sn(p,n)	15	−5.8	1294	51
^{116}Sb	15 m	^{116}Sn(p,n)	15	−5.3	1294	4.3
^{117}Sb	3 h	^{117}Sn(p,n)	8	−2.6	159	39
^{118m}Sb	5 h	^{118}Sn(p,n)	24	−4.7	253	0.048
^{120}Sb	6 d	^{120}Sn(p,n)	32	−3.5	1172	2.2
^{122}Sb	3 d	^{122}Sn(p,n)	5	−2.4	564	20
^{124}Sb	60 d	^{124}Sn(p,n)	5	−1.4	603	46
^{121m}Te	154 d	^{121}Sb(p,n)	57	−2.4	212	16
^{121}Te	16 d	^{121}Sb(p,n)	57	−2.1	573	21
^{123m}Te	120 d	^{123}Sb(p,n)	43	−1.1	159	17

Table 4. (*continued*)

^{120}I	1.3 h	^{120}Te(p,n)	0.09	−3.2	560	17
^{123}I	13 h	^{123}Te(p,n)	0.9	−2.1	159	32
^{124}I	4.2 d	^{124}Te(p,n)	4	−4.0	603	36
^{126}I	13 d	^{126}Te(p,n)	19	−2.9	389	43
^{128}I	25 m	^{128}Te(p,n)	32	−2.0	443	13
^{130}I	12 h	^{130}Te(p,n)	35	−1.2	536	55
^{127m}Xe	69 s	^{127}I(p,n)	100	−1.6	125	7
^{127}Xe	36 d	^{127}I(p,n)	100	−1.3	202	8
^{139}Ce	137 d	^{139}La(p,n)	100	−1.0	166	8

use of accelerator time. Sifting out the 59 cases of $X(\mathrm{p,n})Y$ reactions on even-Z, even-N targets shows a tenuous Gaussian dependence on the reaction Q-value (in MeV) peaked as $\approx 165\,\mathrm{mCi}/\mu\mathrm{A}\exp(-(Q-3.5)/2.1)^2$, if one removes the outliers at major shell closure. No such obvious energy systematics underlie the (p,n) reactions on odd-A targets, indicating the complexity of the many-particle states characterizing the compound nucleus. With the exception of the very important ^{14}N/(p,α) doorway to ^{11}C, most of the other eight (p,α) reactions of Table 6 have a saturation yield of about 5 mCi/μA. Nonetheless, the naturally occuring target abundances make these reactions attractive for the production of ^{7}Be, ^{17}F, ^{55,57}Co and ^{61}Cu.

Second, if one focusses the search for radionulcides with a real potential in biological research, a considerable number emerge in useful

Table 5. Partial list based on biological potential

Radionuclide	Application	References
^{10}C	Regional cerebral blood flow	57
^{14}O	rCBF, oxygen metabolism	58
^{17}F	rCBF	59
^{34m}Cl	Electrolyte balance	
^{45}Ti	Plant metabolism	60
^{52m}Mn	Myocardial perfusion	61
^{52}Mn	Stent activation	62
^{55}Co	Cell death	63
^{60,61,62}Cu	Flow and hypoxia agents	64,65
^{63}Zn	Nutrition	
^{66}Ga	Monoclonal antibodies	66
^{72}As	General labeling	
^{86}Y	PET μ-spheres	67
^{89}Zr	Monoclonal antibodies	68
^{94m}Tc	Bridging PET and SPECT	54,69
^{103}Pd	Specialty brachytherapy sources	
^{124}I	General iodination for PET	

activities, accessible with a small accelerator. The entries in Table 5 reflect this, listing their applications and some representative references.

5. Full circle

A collegial atmosphere pervaded the early years of PET, with cyclotron chemists and imaging scientists free to think ‘outside the box’. This was epitomized by such giants as Paul Harper and Katherine Lathrop at Chicago. Basic research took precedence over ‘pretty pictures’, and a tradition of quantitative measurement of metabolism was born.

PET has now come of age. Re-imbursement for clinical studies, and the turf struggles that follow, threaten to cloud the scientific vision that marked the technique’s origins. Today’s young researchers often find that cyclotron and scanner time are dominated by commercial interests. FDG factories serving cancer clinics are the logical fruit of PET’s success, with a singleness of purpose that is in striking contrast to the 1970’s and 1980’s.

And yet, as commercial cyclotrons are taking over the high volume production of a few PET tracers for routine studies, those surviving academic cyclotrons may well experience a second Renaissance. Freed from the daily responsibilities of making a single agent, the resources and skilled chemists are now liberated to return to basic science, and with it, a fresh look at the chart of the nuclides. Clearly, great strides are being made in the understanding of the subtle kinetics of selective neuroligands, labeled with the ‘conventional’ ^{11}C and ^{18}F. But it is also clear that similar advances await the PET chemist willing to broaden his palette of tracers.

References

1. Curie P, Sklodowska Curie M. Sur une Substance nouvelle Radio-active, contenue dans la Pechblende. *Compt Rend* 1898; **127**: 175.
2. Hevesy G. Radioactive indicators: *Application to Biochemistry, Animal Physiology and Pathology*. Interscience: New York, 1948.
3. Joliot F, Curie I. Artificial production of a new kind of radio-element. *Nature* 1934; **133**: 201.
4. Lawrence EO, Livingston MS. *Phys Rev* 1932; **40**: 19.
5. Van de Graaff RJ. *Phys Rev* 1931; **38**: 1919.

6. Herb RG, Parkinson DB, Kerst DW. *Phys Rev* 1937; **51**: 75.
7. Calvin M, Heidelberger C, Reid JC, Tolbert BM, Yankwich PR. *Isotopic Carbon*. Wiley: New York, 1949.
8. IAEA *Technical Report Series* #136, 1990.
9. Tiller KG. Applications of isotopes to micronutrient studies. *IAEA/FAO Symposium on the Use of Isotopes and Radiation in Research on Soil–Plant relationships*, Colombo Sri Lanka, Dec 1978.
10. Nye PH, Tinker PB. Local movements of solutes in soils. *Solute Movements in the Soil–Root System*. Blackwell: Oxford, 1977.
11. Hanson JE. Influence and application rate on atrazine fate in coarse and fine-textured Wisconsin soils, PhD Thesis, Univ of Wisconsin, 1997.
12. Wagner HN. *Principles of Nuclear Medicine*. WB Saunders and Co: Philadelphia, 1968; 15.
13. Harper PV, Lathrop KA, Gottschalk A. In *Radioactive Pharmaceuticals*, Andrews GA, Kniseley JW, Wagner HN (eds). US Atomic Energy Commission, 1966.
14. Root JW, Krohn KA. Short-lived radionuclides in chemistry and biology. *Advances in Chemistry Series,* Vol. **197**, Amer Chem Soc: Washington DC, 1981.
15. Thomas J, Meeks JC, Wolk CP, Shaffer CP, Austin SM, Chien W-S. *J Bacteriol* 1977; **129**: 1545.
16. Nickles RJ, Kiuru AJ, Schuster SM, Holden JE. A catalytic generator for the production of $H_2^{14}O$ and $H_2^{15}O$. *Prog Nucl Med* 1978; **4**: 72.
17. Powell J, Guo FQ, Haustein PE, *et al*. In Duggan JL and Morgan IL (eds). BEARS: a radioactive ion beam initiative at LBNL. *AIP Conference Proceedings*, Vol. **475**, Applications of Accelerators in Research and Industry, *Am Inst Phys*: CP475, 1999; 318.
18. Decrock P, Delbar Th, Duhamel P, Determination of the $^{13}N(p,\gamma)^{14}O$ reaction cross section using a ^{13}N radioactive ion beam. *Phys Rev Lett* 1991; **67**: 808.
19. Rehm KE, Paul M, Roberts A, *et al.* The astrophysical reaction rate for the $^{18}F(p,\alpha)^{15}O$ reaction. *Phys Rev C* 1996; **53**: 438.
20. General Electric Co, *Chart of Nuclides* (12th edn). Schenectady: New York, 1977.
21. W.D. Myers and W.J. Swiatecki, Nuclear masses and deformation. *Nucl Phys* 1966; **81**: 1.
22. Friedlander G, Kennedy JW, Macias ES, Miller JM. *Nuclear and Radiochemistry*. (3rd edn). Wiley: New York, 1981; 41.
23. Blann M. *Corrections to Overlaid ALICE*. University of Rochester, Nuclear Structure Research Lab, UR-NSRL-181, 1978.
24. Landolt-Bornstein, Numerical Data and Functional Relationships in Science and Technology, New Series, Vol. 5. Hellewege K-H (ed),

Q-values and Excitation Functions of Nuclear Reactions, Part b, Keller KA, Lange J, Munzel H, Pfennig G (eds), Springer: Berlin, 1973.

25. Schaarf W. Particle Accelerators. *Applications in Technology and Research*. Research Studies Press, Ltd., Wiley: New York, 1989.
26. Scholten B, Kovacs Z, Tarkanyi F, Qaim SM. Excitation functions of ^{124}Te(p,xn) ^{124,123}I reactions from 6–31 MeV with special reference to the production of ^{124}I at a small cyclotron. *Appl Rad Isotopes* 1995; **46**: 225.
27. Sheh Y, Koziorowski J, Balatoni J, Lom C, Dahl JR, Finn RD. Low energy cyclotron production and chemical separation of 'no-carrier-added' iodine-124 from a Reusable enriched tellurium-124 dioxide/aluminum Solid Solution Target. *Radiochim Acta* 2000; **88**: 169.
28. Watson IA, Waters SL, Silvester DL. Excitation functions for the reactions producing ^{121}I, ^{123}I and ^{124}I from Irradiation of Natural Antimony with ^{3}He and ^{4}He Particles with Energies up to 30 MeV. *J Inorg Nucl Chem* 1973; **35**: 3047.
29. Reischl G, Roesch F, Machulla HJ. Production of iodine-124 with a new target system at a low energy cyclotron. *J Nucl Med* 2000; **41**: 252P.
30. Snowdon SC. Excitation curve for protons in the reaction ^{19}F(d,p) ^{20}F. *Phys Rev* 1950; **78**: 299.
31. Nickles RJ and Hichwa RD. A digital leaky integrator. *Nucl Instr Meth* 1979; **158**: 609.
32. Hichwa Rd, Watkins GL, Ponto LL, Cyclotron produced ^{18}F fluoride: a target's view of the beam. *J Nucl Med* 2001; **42**: 18P.
33. Excergen Corp., Watertown, MA.
34. Schueller MJ. An investigation of $^{10}CO_2$ and $H_2^{14}O$ as cerebral blood flow tracers. *PhD Thesis*, University of Wisconsin, 2001.
35. Aho K, Light emission during cyclotron bombardment of gases used in radionuclide production. *PhD Thesis*, Abo Akademi, Abo, 1998.
36. Solin O, Interaction of high energy charged particles with gases, *PhD Thesis*, Abo Akademi: Abo, 1988.
    Heselius S-J, Studies of density reduction in gas targets, *PhD Thesis*, Abo Akademi: Abo, 1986.
37. LND Inc., 3230 *Lawson Blvd*. Oceanside: New York, 11572.
38. Knoll GF. *Radiation Detection and Measurement* (2nd edn). Wiley: New York, 1979; 487.
39 Beyer G-J, Pimental G. Physiocochemical and radiochemical aspects of separation of radioiodine from TeO_2-targets. *Radiochim Acta* 2000; **88**: 175.
40. Keithley Instruments Inc., 28775 Aurora Rd., Cleveland OH 44139. Model CTM-05/A and DAS-801.
41. Nickles RJ, Votaw JR. An extended range well counter. *IEEE Trans Nucl Sci* 1985; **32**(1): 60.

42. Nickles RJ, Solin OH. A wide-range flexible gamma probe. *Appl. Radiat Isotopes* 1992; **43**: 1169.
43. Nickles RJ, Solin OH, Harparaanta M, DeJesus OT. A flow-through detector for nano-curie activities encountered in HPLC analysis of PET tracer metabolites. *IEEE Trans Nucl Sci* 1992; **39**: 2316–2321.
44. Keithley Instruments, Inc., 28775 Aurora Rd, Cleveland OH 44139, Model 6517A.
45. Hamamatsu Photonics Corp, 360 Foothill Road, PO Box 6910, Bridgewater, NJ 08807, Model S2281-01.
46. Fluke Corp., PO Box 909-, 6920 Seaway Blvd, Everett WA 98203, Model 79.
47. Nickles RJ, Christian BT, Nunn AD, Stone CK. Cyclotron production of high purity Tc-94m by *in situ* sublimation. *J Label Compd Radiopharm* 1993; **32**: 447–448.
48. Roesch F, Novgorodov AF, Qaim SM. Thermochromatographic separation of ^{94m}Tc from enriched molybdenum targets and its large scale production for nuclear medicine application. *Radiochim Acta* 1994; **64**: 113.
49. Beyer GJ, Pimental G, Solin O, *et al*. Production of ^{123}I for medical use with small accelerators. *Isotopenpraxis* 1988; **24**: 297.
50. Nickles RJ and Au YF. The oxygen clock, a dual tracer physiological timer. *Phys Med Biol* 1975; **20**: 54.
51. Cotton FA, Wilkinson G. *Advanced Inorganic Chemistry* (4th edn). Wiley: New York, 1980; 989.
52. Zhang J-Z, Boorse SR, Halpern BL, Schmitt JJ, Gai M. Novel targets for radioisotope generation made by the jet vapor deposition process. In Link JM, Ruth TJ (eds). *Proceedings of the Sixth Workshop on Targetry and Target Chemistry*, Vancouver, 1995; 147.
53. Friedlander G, Kennedy JW, Macias ES, Miller JM. *Nuclear and Radiochemistry* (3rd edn). Wiley: New York, 1981; 290.
54. Nickles RJ, Nunn AD, Stone CK, Christian BT. Technetium-94m-Teboroxime: synthesis, dosimetry and initial PET imaging studies. *J Nucl Med* 1993; **34**: 1058.
55. Stone CK, Christian BT, Nickles RJ, Perlman SB. Technetium-94m methoxy isobutyl isonitrile: dosimetry and resting cardiac imaging with positron emission tomography. *J Nucl Cardiol* 1994; **1**: 425.
56. Nickles RJ. Production of a broad range of radionuclides with an 11 MeV proton cyclotron. *J Label Compd Radipharm* 1991; **30**: 120.
57. Law I, Jensen M, Holm S, Nickles RJ, Paulson OB, Using $^{10}CO_2$ for single subject characterization of the stimulus frequency dependence in visual cortex – a nover PET tracer for human brain mapping. *J Cereb B1 Flow Metab* 2001; **21**: 1003–1012.

58. Nickles RJ, Jensen M, Paans AMJ, Holm S, Schueller MJ, Vaalburg W. Doppler broadening revealing the chemical environment following oxygen-14 decay. *Radiochimica Acta* 2000; **88**(3–4), 189–193.
59. Roberts AD, Dabbs KA, Schueller MJ, Dick DW, Nickles RJ. Production of the short-lived flow tracer fluorine-17 fluoromethane from proton irradiation of neon. *J Nucl Med* 2000; **41**: 243P.
60. Saitoh K, Inoue K, Kawamura M, Ishiwata K, Ido T, Kimura S. Studies on the relationship between the biodistribution of ^{45}Ti–AsA in the rat kidney and renal function. *Cyric Annual Report*, 1987; 182.
61. Daube ME, Nickles RJ. Comparison of positron-emitting myocardical perfusion agents. *J Nucl Med* 1983; **24**: 119.
62. Hehrlein C, Gollan C, Donges K, *et al*. Low-dose radioactive endovascular stents prevent smooth muscle cell proliferation and neointimmal hyperplasia in rabbits. *Circ* 1995; **92**: 1570.
63. Jansen HML, Pruim J, van de Vliet AM *et al*. Visualization of damaged brain tissue after ischemic stroke with cobalt-55 positron emission tomography. *J Nucl Med* 1994; **35**: 456.
64. Green MA, Mathias CJ, Welch MJ, *et al*. Copper-62-labeled pyruvaldehyde Bis(N^4-methylthiosemicarbazonato) copper (II): synthesis and evaluation as a positron emission tomography tracer for cerebral and myocardial perfusion.
65. Martin CC, Oakes TR, Nickles RJ. Small cyclotron production of Cu-60 PTSM for PET blood flow measurements. *J Nucl Medi* 1990; **31**: 815.
66. Koziorowski J, Finn RD, Pentlow KS, *et al*. Preliminary results on the production of ^{66}Ga, a non-conventional positron emitter. *Eighth Workshop on Targetry and Target Chemistry, St. Louis*, 1999.
67. Brockman J, Roesch F, Herzog H, Stolz B, Bruns C, Stocklin G. *In vivo* uptake kinetics and dosimetric calculations of ^{86}Y-DTPA-octreotide with PET as a model for potential entotherapeutic octreotids labelled with ^{90}Y. *J Lab Compd Radiopharm* 1995; **37**: 519.
68. Link JM, Krohn KA, Eary JF, *et al*. ^{89}Zr for antibody labelling and positron tomography. *J Label Compd Radiopharm* 1986; **23**: 1296.
69. Qaim, SM. Production of high purity ^{94m}Tc for positorn emission tomography studies. *N Med Biol* 2000; **27**: 323.

